Journal of Non-Crystalline Solids 636 (2024) 123017

Contents lists available at ScienceDirect

Journal of Non-Crystalline Solids

journal homepage: www.elsevier.com/locate/jnoncrysol

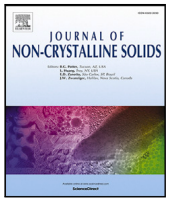

Molecular dynamics simulations of SiS_2-Li_2S-LiI fast ion glasses: Increase of conductivity is driven by network atoms

M. Micoulaut

Sorbonne Université, Laboratoire de Physique Théorique de la Matière Condensée, CNRS UMR 7600, 4 Place Jussieu, 75252 Paris Cedex 05, France

ARTICLE INFO

Keywords:
Glasses
Molecular dynamics simulations
Chalcogenides
Amorphous electrolytes

ABSTRACT

We investigate the role of an alkali additive in order to understand the effect of structure on the dynamic and electric properties of amorphous electrolytes that can be used in future all solid-state batteries. Targeted glasses are $0.6Li_2S$-$0.4SiS_2$ and a "doped" $0.42Li_2S$-$0.28SiS_2$-0.3LiI ternary which is known to display interesting conductivity levels (10^{-3} Ω^{-1} cm^{-1}). We first set up a force field for the ternary system, and build on a recent potential [Phys. Rev. B **107**, 214205 (2023)] which is able to describe appropriately lithium thiosilicates. Results indicate an increased depolymerization of the thiosilicate network structure upon LiI addition that is visible in the tetrahedral Si speciation which alters stress distribution and free volume in the glass. The calculated diffusivities reveal that network dynamics is substantially increased upon LiI addition, manifests by a breakdown of the channel dynamics of Li motion, and contributes to the overall conductivity.

1. Introduction

The Li-ion technology has emerged in order to provide solutions to worldwide ever-increasing demand on energy and power density batteries which are in use in portable electronics such as laptop computers, smartphones or electric scooters. Central to this development is also the growing need of fast ion conducting batteries for the transition towards electric vehicle [1,2]. A major roadblock is the thread of safety hazard because of the presence of flammable polymeric liquid electrolytes and the possibility of having shortcuts initiated by dendritic Li growth between the electrodes [3]. Alternative and safe solutions have, therefore, to be imagined. In order to improve of the component's safety, solid electrolytes have now received growing interest, and amorphous or glassy electrolytes [4] are now also considered as promising possibilities. The use of a solid state electrolyte now also opens the perspective to use Li metal electrodes instead of Li oxide based ones such as the popular $LiCoO_2$, and this should also increase the power density of the batteries.

Unlike crystalline polymorphs, glasses have also the advantage of being easily recyclable, and are easy to produce [5]; they display rather good thermal and mechanical stability, and as the number of possible compositions is infinite, a continuous improvement of the batteries' performances can be imagined with the use of targeted multi-component systems. In this context, sulfides have received considerable attention due to the increased polarizability of sulfur, and measured conductivity can be as much as $\sigma \simeq 10^{-3}$ Ω^{-1} cm^{-1} [6] which makes them attractive for solid state batteries.

An interesting means to increase the ionic conduction is to bring in an additive which can represent up to 50% of the glass composition. In sulfides, these have usually been alkali halides such as LiI and their addition into modified sulfur-based glasses has led to conductivity levels up to $2 \times 10^{-3}\,\Omega^{-1}$ cm^{-1} for e.g. P_2S_5-SiS_2-Li_2S-LiI [7,8]. Such measurements are rather old but have displayed promising levels of conduction at room temperature: Li_2S-B_2S_3-LiI (10^{-3} Ω^{-1} cm^{-1} [9]), Li_2S-(Ge,Si)S_2-LiI (0.8×10^{-3} Ω^{-1} cm^{-1} [10]), 45LiI-37Li_2S-18P_2S_5 (10^{-3} Ω^{-1} cm^{-1} [11]). Among the possible lithium halides, it seems that one has $\sigma_I > \sigma_{Br} > \sigma_{Cl}$ [12] so that the addition of LiI has been almost systematically preferred when attempting to increase the conductivity level. Not much further increase in ionic conduction has been achieved since then, the main drawback being the rather poor glass-forming tendency of such multi-component alloys which need the use of extremely high quenching rates, typically 10^6 K/s [13], or a direct liquid nitrogen quench [7]. Recently, mechanical ball milling techniques have emerged and these have permitted to considerably extend glass-forming ranges of chalcogenides [14]. It is, therefore, tempting to reconsider such doped glasses from atomic scale models in order to establish and substantiate structure–property relationships, as e.g. performed on a parent system (Li_2S-P_2S_5-LiI [15]).

Here, we focus on two glassy systems using molecular dynamics simulations: a "reference" $0.6Li_2S$-$0.4SiS_2$ (LS) composition and a modified $0.7(0.6Li_2S$-$0.4SiS_2)$-0.3LiI = $0.42Li_2S$-$0.28SiS_2$-0.3LiI (LSI). The interest in this kind of ternary system is motivated by the fact that

E-mail address: matthieu.micoulaut@sorbonne-universite.fr.

https://doi.org/10.1016/j.jnoncrysol.2024.123017
Received 20 January 2024; Received in revised form 15 April 2024; Accepted 3 May 2024
Available online 15 May 2024

alkali additives such as LiI or LiCl usually lead to an increase of the ionic conductivity by increasing the number of charge carriers, and the aforementioned LSI glass is, in fact, known to display an important level of ionic conduction (2.0×10^{-3} Ω^{-1} cm^{-1} [7,16]) that is substantially increased with respect to the LS counterpart (0.5×10^{-3} Ω^{-1} cm^{-1} [7, 16–18]). The glass-forming range of the SiS_2-Li_2S-LiI ternary has been studied along a select number of compositional joins [12], i.e. (1-x)(0.4SiS_2-0.6Li_2S)-xLiI and (1-x)(0.5SiS_2-0.5Li_2S)-xLiI but results [16] focused essentially on electrical properties and only a limited number of structural properties were obtained from infrared and nuclear magnetic resonance spectroscopy [12] but real space properties such as those accessed from scattering experiments (X-ray or neutron) or from atomic simulations are still lacking. To this end, we use a recently developed classical force-field that has been established for the crystalline (Li_2SiS_3) and amorphous phases of the Li_2S-SiS_2 system [19]. It is able to correctly reproduce the structural properties of the glass (experimental structure functions such as structure factor and pair correlation functions [18,20]), and the crystal properties [21,22] (cell lengths, densities at zero pressure), together with other different properties. We extend the potential to account for the LiI additive by adding a fractional iodine charge, and a strongly repulsive interaction at short distances that is determined from related crystalline phases such as LiI and SiI_4.

Results indicate that the addition of (LiI) into a Li_2S-SiS_2 solid electrolyte glass contributes to various effects in terms of structure with an obvious increased (entire) depolymerization and the replacement of certain sulfur by iodine atoms in the first coordination shell of silicon. The dynamics suggests an increased motion for the network species (i.e. Si and S) in the modified liquids that we interpret from the increased depolymerization of the structure which also leads to a vanishing of the channel dynamics observed in the "reference" system. This results in an increased contribution of Si and S atoms to the overall conductivity. The doping is, furthermore, accompanied by a substantial increase of free volume that will facilitate conduction and by an evolution of local stresses whose spatial fluctuations tend to reduce. These numerical results highlight the importance of doping which is known to contribute to the presence of additional charge carriers. Atomic simulations provide here a detailed picture in which additives act also in a more complex or subtle way in terms of structure–property relationships.

2. Simulation details

2.1. Preparing glassy systems

The considered systems are made of 3000 atoms (Fig. 1). The initial configurations have been obtained from a starting Li_2SiS_3 one [19] and atoms have been randomly selected and replaced in order to fulfill the desired stoichiometry, i.e. one has $N_{Li} = 1200$, $N_{Si} = 400$ and $N_S = 1400$ for the reference LS system, and $N_{Li} = 1266$, $N_{Si} = 312$, $N_S = 1088$ and $N_I = 334$ for the doped (LSI) one. The starting density of both systems has been taken as $\rho_0 = 0.051$ Å^{-3} = 1.82 g cm^{-3} [18] corresponding to $L = 38.87$ Å.

Classical molecular dynamics simulations with a parametrized Buckingham-type potential (see below) has been used, together with a Verlet algorithm with 1 fs time step for the integration of the equations of motion in NPT (for the quench) or NVT Ensemble (for the analysis):

$$V_{ij}(r) = A_{ij} \exp\left(-r/\rho_{ij}\right) - \frac{C_{ij}}{r^6} + \frac{q_i q_j}{4\pi\epsilon_0 r}, \quad (1)$$

where r is interatomic distance, A_{ij}, ρ_{ij}, and C_{ij} are parameters, q_i are the charges (in e units), and ϵ_0 is the permittivity of vacuum. i and j refer to the type of two distinct atoms. After an initial run at high temperature (2000 K) and zero pressure over 100 ps in order to loose the memory of the unphysical initial configurations, the liquids have been quenched with cooling rate 1 K/ps to room temperature (300 K)

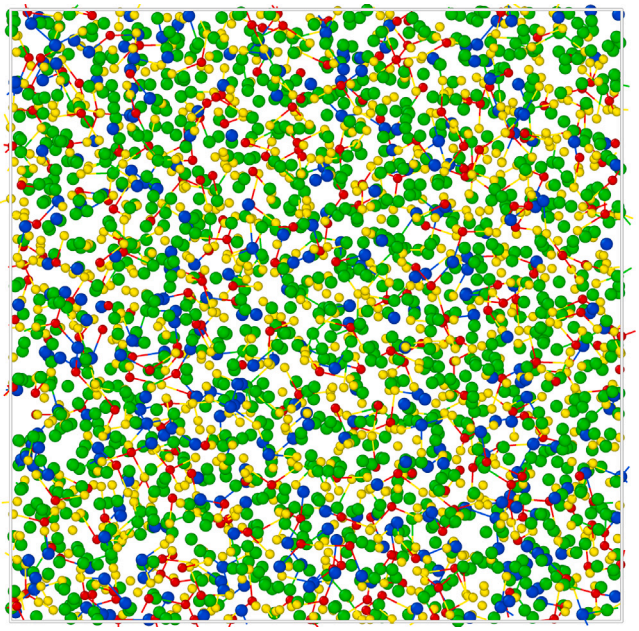

Fig. 1. Snapshot of the doped glass 0.42Li_2S-0.28SiS_2-0.3LiI (LSI). Blue and green atoms are iodine and lithium, respectively. The thiosilicate network structure is represented by red and yellow.

in NPT at zero pressure. Such configurations have then be heated back in NVT at different target temperatures used for the analysis of the dynamics in the liquid state. Statistical analysis have been performed over 1 ns. The resulting density at 300 K for the reference LS system is close to the experimental one [18] as we found $\rho_0 = 1.83$ g cm^{-3}. For the LSI compound, we are not aware of any measured density for this particular composition but acknowledge the fact that the glass at zero pressure obtained after the quench has a density of $\rho_0 = 1.83$ g cm^{-3} that is very close to the one obtained for the reference system and typical of other modified multi-component thiosilicates [23] but somewhat larger than densities measured for parent (chlorine) compositions, (1-x)[0.5SiS_2-0.5Li_2S]-xLiCl (1.45–1.55 g cm^{-3} [24]).

2.2. Setting up the additional potential parameters

In order to take into account the presence of LiI, there is need to parametrize four additional interactions: Si–I, S–I, I–I, and Li–I. Since $q_{Li} = 0.6e$ [19], we used $q_I = -0.6e$ together with parameters fitted to recover the structural properties of the elementary cell of crystalline LiI (cubic Fm-3m, $a = 6.00$ Å [25,26]), and SiI_4 (cubic Pa-3, $a = 11.99$ Å [27]). We are not aware of any S–I compounds which are known to be unstable at ambient conditions, and exist only as other chalcohalides under the form of complex cations [28]. Since the S–I bond distance in such compounds and related salts is of the order of 2.30–2.40 Å [28,29], i.e. similar to Si–I, we will assume $V_{SI}(r) = V_{SiI}(r)$.

We fit empirically such crystal structure data within the general utility lattice program (GULP) and zero forces [30,31], in conjunction with a relaxation technique and a vibrational eigenmode calculation that permits to select among fitted parameters those which lead to stable crystalline structures at ambient temperature. Within this fitting procedure, one minimizes a weight function F,

$$F = \sum_{k=1}^{M} \left[C_{calc}(k) - C_{obs}(k)\right]^2 \quad (2)$$

with M observables $C_{obs}(k)$ being the atomic coordinates of the crystalline elementary cells with zero forces. The fitting procedure, i.e., the

Table 1
Buckingham parameters of Eq. (1) that describe crystalline LiI and SiI_4, and are used in addition to (S,Li,Si) pairs obtained for SiS_2-Li_2S glasses. As for the latter pair potential [19], we used $q_S = -2q_S i = -2.4$e, $q_{Li} = 0.6$, and for the LSI we used $q_I = -0.6$e.

Atom i	Atom j	A_{ij} (eV)	ρ_{ij} (Å)
I	I	14472451.0	0.161
I	Li	213 890.0	0.190
I	Si	7096.5	0.263
I	S	7096.5	0.263

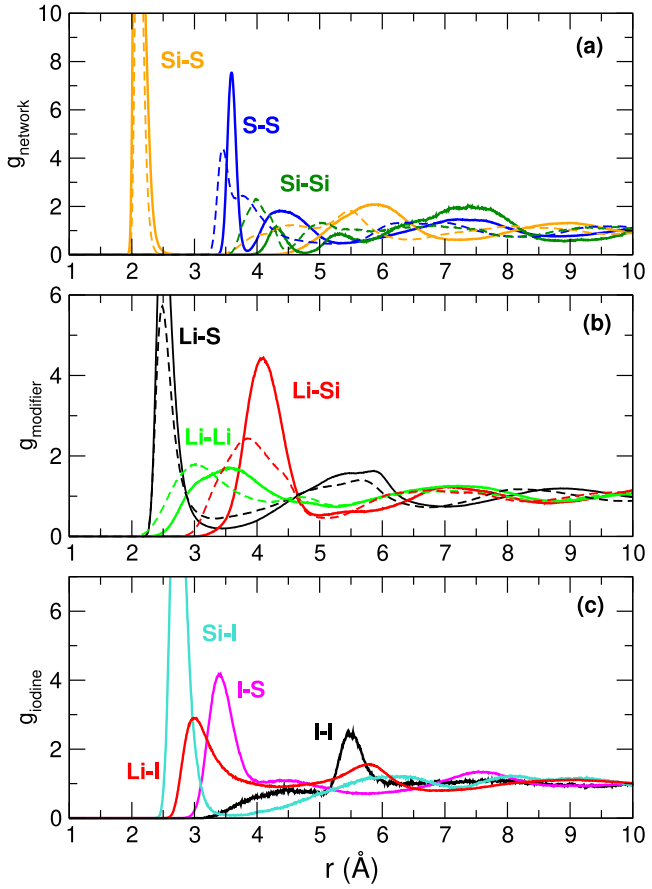

Fig. 2. Partial pair correlation functions of $28SiS_2$-$42Li_2S$-30LiI glasses, presented in termes of network species (a), Li-related species (b) and iodine-related species (c). Broken lines correspond to results for $40SiS_2$-$60Li_2S$.

variation of the potential parameters so as to get the positions with zero forces, stops when the energy gradient becomes lower than a certain value (typically 0.01 a.u.). In the GULP procedure, this strategy can be refined by requesting that with a set of parameters (A_{ij}, ρ_{ij} and C_{ij}) the determined 3N vibrational eigenmodes (phonons) of the structure (i.e. the eigenvalues of the dynamical matrix [32]) are all positive. This ensures that second derivatives of V_{ij} with respect to the atoms in Cartesian space (i.e., the force constant matrix) are positive and lead to stable vibrations. The lowest three modes are zero at the center of the Brillouin zone (Γ point), and these correspond to the pure translation of the crystal lattice, identified with the acoustic branch.

We kept the determined Li–Li interactions [19] of the Li_2SiS_3 glass, and maintained for simplicity all coefficients C_{ij} to zero, as for most of these parameters in Li_2SiS_3. Using this strategy, parameters for the iodine related interactions could be determined and are displayed in Table 1, to be used for the present SiS_2-Li_2S-LiI system.

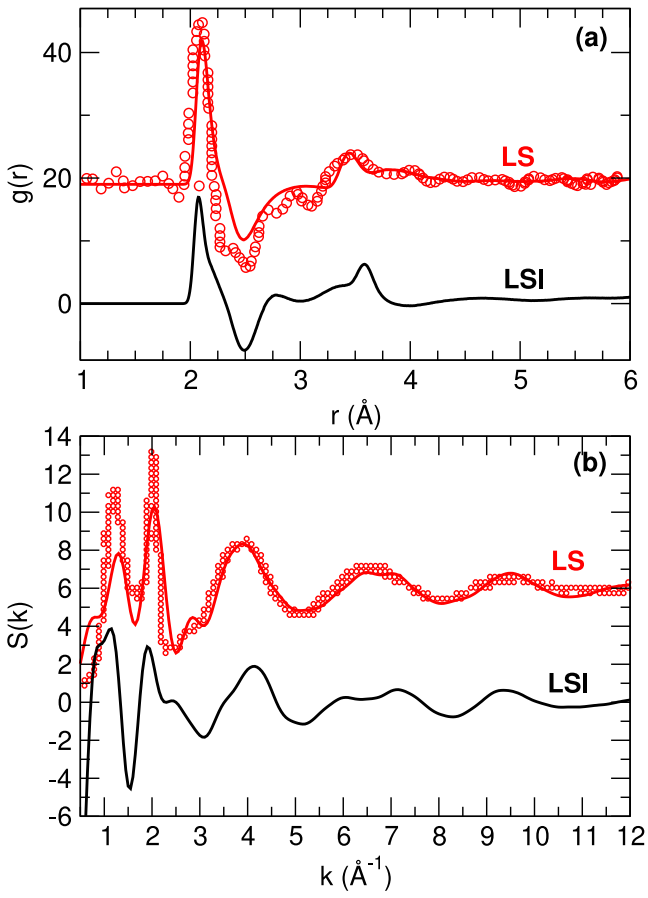

Fig. 3. Calculated neutron pair correlation function $g(r)$ (a) and structure factor $S(k)$ (b) of LS (red) and LSI glasses (black). The circles are digitized data from neutron scattering experiments [18]. Data sets have been shifted for a clearer presentation.

3. Results

In the forthcoming, we provide the structural properties of such glasses and describe how the addition of LiI induces changes in transport and electrical properties.

3.1. Structure

Fig. 2 displays the partial pair correlation functions for LS (broken lines) and LSI (solid lines). Their neutron weighted combination leads to the total pair $g(r)$ displayed in Fig. 3a which is compared to data from neutron scattering of LS glasses [18]. Here we have used b_S = 2.847 fm, b_{Si} = 4.149 fm, $b_{Li} = -1.90$ fm and b_I = 5.28 fm as coherent neutron scattering lengths. Results indicate that the main experimental features in real space and reciprocal space are obtained for the present system. It is found, indeed, that the main peak at 2.1 Å and a secondary principal peak at 3.5 Å are recovered from the simulations for the LS system (Fig. 3a), and reproduced in terms of intensity and position. Corresponding data for the ternary have not been reported in the literature, but the simulation suggests that upon LiI addition, the main peak reduces in intensity, together with a shift to larger distances (3.6 Å) for the secondary peak, the evolution being associated with an increased contribution of the S–S partial (Fig. 2a) and the presence of a typical distance involved in S–I correlations (Fig. 2c). The dominant motif continues to be tetrahedral Si with a Si–S bond length at 2.1 Å (Fig. 2a) similar to the LS reference system. The same conclusion can be drawn for the other network-forming partials, i.e. S–S (d_{S-S} = 3.53 Å) and Si–Si (d_{Si-Si} = 4.14 Å), and this highlights the fact that the

tetrahedral character of the network is preserved with the apex formed by the Si–S bond and the edge by the S–S one. This is, indeed, confirmed by the obtained value of the tetrahedral ratio $\delta = d_{S-S}/d_{Si-S}$ [33] that is here equal to 0.610, i.e. very close to the value $\sqrt{3/8} = 0.612$ found for a regular tetrahedron, as in other chalcogenides [34]. Noteworthy is the fact that the addition of LiI induces in the S–S correlation a secondary peak at ≃4.5 Å that is now well separated (with respect to the reference LS), and related to the presence of dominant Q^0 units (see below). Finally, one acknowledges the absence of possible polysulfide S–S chain fragments which appear as defects in sulfide electrolytes and act as trapping sites for alkali ions while also leading in select cases to preferential pathways for ionic conduction [35]. Here, we note that no typical pre-peak is detected in the simulated S–S pair correlation functions (Fig. 2a). This typical pre-peak is present in GeS_2 network formers [36] at the distance of 2.22 Å [37], and also in sodium thiogermanates [38]. The present simulations, thus, suggest that in both investigated thiosilicate glasses, such features are absent.

A comparison of the obtained simulations in reciprocal space also permits to assess the validity of the force field for LS systems (Fig. 3b) by comparing with the measured structure factor $S(k)$ from digitized neutron scattering experimental data [18]. While the simulations of the LS glass replicate all experimental peaks, the first peak displays an obvious reduced intensity but a near correct position (1.3 $Å^{-1}$), while all other positions and intensities of the principal peaks at 2.1 $Å^{-1}$, 3.9 $Å^{-1}$ and 6.5 $Å^{-1}$ are reproduced. This indicates that most of the MRO elements of the structure are accurately described. With LiI addition, some longer correlating distances must appear as a typical peak builds up in the small k region.

The second major outcome is that iodine enters into the first coordination shell of Silicon as it sometimes happen for Group IV chalcohalides [39]. Here, although the first Si–I correlating distance is found at r ≃2.72 Å, i.e. slightly larger than the Si–S bond distance, at the minimum of g_{SiS} (3.0 Å) the evaluation of the running Si-based coordination numbers $n(r)$ shows that the Si–S coordination number reduces (Fig. 4) from $n_{Si-S} = 4.0$ in the reference LS glass (broken curve) to 3.3 for the LSI one, i.e. slightly larger than what might be expected if all iodine atoms would take part in the first coordination shell ($n_{Si-S} = 3.0$). Although this scenario might be possible on stoichiometry grounds since N_I and N_{Si} are similar (334 and 312 atoms, respectively), we have calculated that at the cut-off distance (3.0 Å), the population of Si atoms is made of ≃75% tetrahedra having four Si–S bonds and 25% Si having three Si–S and one Si–I bond. This leads to a global coordination number n_{Si-S} slightly larger than three in LSI. The residual iodine atoms which do not participate in the Si first coordination shell remain in the vicinity of Li atoms as suggested from the principal peak observed at a somewhat larger distance than the Si–S one in the corresponding Li–I partial (Fig. 2c). These iodine based correlations furthermore indicate that Li–I bondings are present in the glass, unlike in corresponding thiophosphates [15] since the corresponding Li–I distance (3.06 Å) is found to be much shorter than in these glasses (6.0 Å). This underscores the fact that the effect of additional "free" lithium cations able to depolymerize the starting LS network might be reduced. Similarly, there is no preferential short bond distance of the I–I bond distance which would indicate a possible iodine clustering. Instead, one acknowledges a long distance correlation (5.5 Å) between the diluted I^- ions in the glassy network.

Finally, the Li-related partials (Fig. 2b) suggest that the bonding distances remain nearly unchanged between the reference LS and the doped LSI, and one finds d_{Li-S} = 2.49 Å, d_{Li-Li} = 3.10 Å (2.94 Å in the reference system), and d_{Si-Li} = 3.92 Å.

An addition analysis of the structure uses the Q^n terminology which represents the population of Si tetrahedra having n bridging sulfur (BS), i.e. sulfur atoms connecting two tetrahedra between them. The base network (silica or SiS_2) is made of 100% Q^4 units, whereas highly depolymerized glasses usually display a near 100% fraction of Q^0 units represented by "isolated" Li_4SiS_4 tetrahedra. Such Q^n populations can

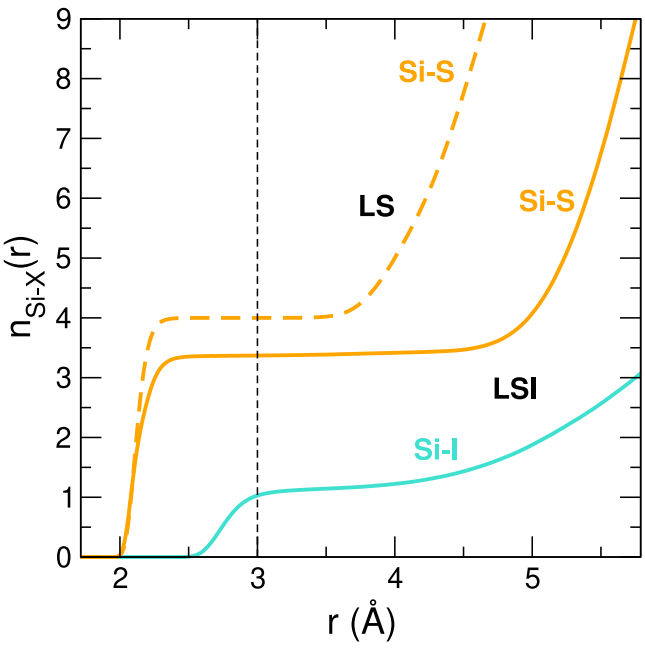

Fig. 4. Calculated Si partial coordination numbers $n_{ij}(r)$ as a function of correlating distance in LS (broken line) and LSI (solid lines). The vertical broken curve corresponds to the minimum of the Si–S partial pair correlation function.

Table 2
Calculated fraction of Q^n distribution (in %)) in LS and LSI glasses, and compared to other compositions in the Li_2S-SiS_2 system [19] and to models from the literature.

	Q^4	Q^3	Q^2	Q^1	Q^0
LSI				6.4	93.1
LS		10.7	26.8	42.0	20.5
Li_2SiS_3 [19]	5.8	20.7	35.4	30.6	7.5
Topological model LS [40]	0.1	0.1	0.1	99.6	
Ideal chemical model				100.0	

be measured by solid state nuclear magnetic resonance (^{29}Si NMR [13, 41,42]). In thiosilicates, and in contrast with alkali silicates [43], the difficulty of establishing such populations arises from the small number of reference crystalline phases (Li_2SiS_3 and Li_4SiS_4) in comparison with corresponding oxides, and small chemical shift anisotropies which do not permit to completely distinguish between various Q^n species. As a result, the addition of Li_2S into SiS_2 leads only to small variations in the ^{29}Si chemical shift [44] so that the Q^n distribution with composition or temperature is almost unknown in thiosilicates.

The calculated Q^n distribution of the LS and LSI glasses reveals a profound change upon LiI addition (Table 2) with a nearly complete depolymerized structure for LSI, whereas the LS reference glass contains fractions of various Q^n tetrahedra, except Q^4. It is important to note that for LSI the notion of Si tetrahedra is not fully compatible with the one used in the literature [43] since some of the tetrahedra in LSI contain some Si–I bonds. Here, the Q^n species in LSI glasses are enumerated according to the number of Si-X-Li correlations around a central Si atom, irrespective of the nature of the non-bridging X (X=S,I). For the reference LS system and when one compares with the $50Li_2S$-$50SiS_2$ (Li_2SiS_3 [19]), we note a substantial increase of Q^1 and Q^0 units, as it should be. The additional Li ions lead, indeed, to more and more non-bridging sulfur atoms having in their vicinity a Li ion. These statistics are rather different from those proposed in idealized models for which the statistics is essentially 100% Q^1. The LSI glass is found to display an obvious increased depolymerization with a near network containing ≃100% Q^0 species and some Q^1-Q^1 dimers. This is consistent with the fact that for the LSI composition

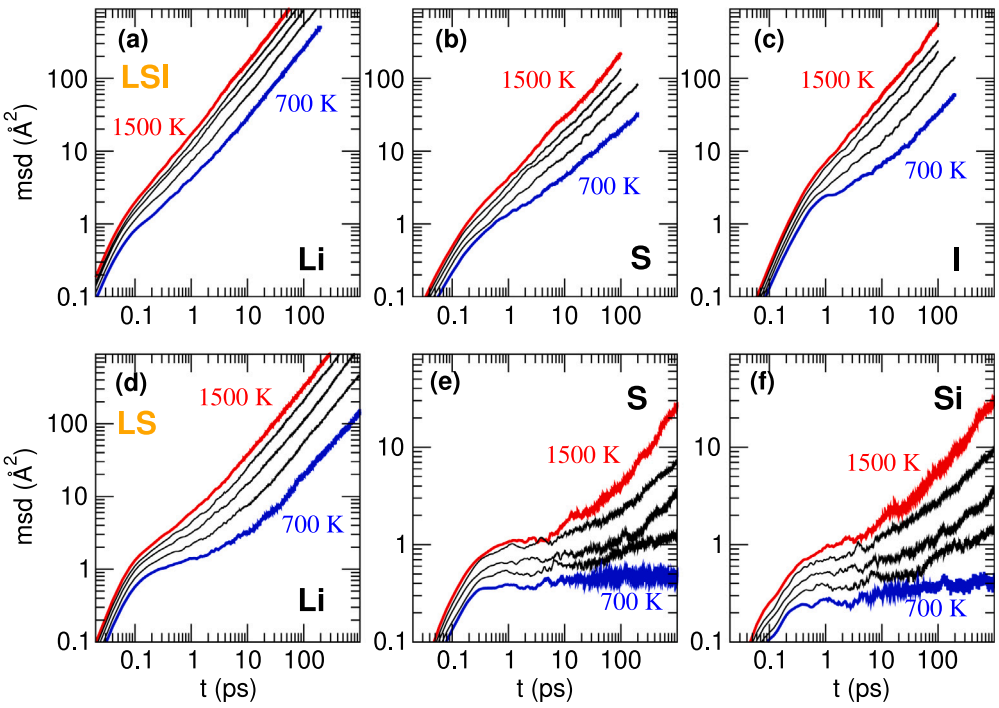

Fig. 5. Calculated mean-square displacement at different target temperatures of Li (a), S (b) and I (c) atoms in LSI liquids, and Li (d), S (e) and Si(f) LS liquids. Red and blue curves correspond to the 1500 K and 700 K isotherms, respectively. Black curves correspond to the intermediate temperatures (1300 K, 1100 K and 900 K).

Table 3
Calculated diffusivities (in 10^{-5} cm^2 s^{-1}) of LS and LSI liquids at different temperatures. See also Fig. 6.

System		1500 K	1300 K	1100 K	900 K	700 K
LSI	D_S	3.682(1)	2.249(7)	1.566(2)	0.766(4)	0.311(1)
	D_{Si}	2.841(7)	1.676(4)	1.194(3)	0.578(0)	0.191(2)
	D_{Li}	27.0410	20.031(7)	14.316(2)	9.015(9)	4.329(7)
	D_I	9.234(1)	5.582(6)	3.855(1)	1.709(5)	0.541(2)
LS	D_S	0.078(2)	0.031(1)	0.016(4)	0.019(1)	
	D_{Si}	0.096(6)	0.046(5)	0.018(1)	0.009(7)	
	D_{Li}	5.363(1)	3.442(7)	1.961(0)	0.881(7)	0.309(4)

(0.42Li_2S-0.28SiS_2-0.30LI), the Li:Si atomic ratio is 4.07:1 which must promote the presence of four non-bridging atoms around Si, i.e. n = 0. The complete depolymerization of the LS glass by the additive is also detected from the near vanishing of the first correlating Si–Si distance (4.0 Å) in the associated pair correlation function (Fig. 2a) which reduces to a small peak at 4.25 Å that corresponds to the Si–Si distance of the Q^1-Q^1 dimers.

The picture that emerges is that the addition of LiI leads to various effects in terms of structure. The LiI additive partially dissociate into the LS base network and contributes to the replacement of certain sulfur atoms in the first coordination shell of Si that also leads to changes in the Q^n distribution and the pair correlation functions.

4. Diffusivity and conductivity

Our main interest is to determine whether the addition of LiI induces an increase in conductivity, and to relate this increase to some structural features driven by composition.

4.1. Diffusivity

To this end, we first investigate the dynamics of the corresponding liquids by focusing on the mean square displacement (msd) of the atoms, defined from the positions $\mathbf{r}_j(t)$ at time t

$$\langle r_k^2(t)\rangle = \left\langle \frac{1}{N_k}\sum_{j=1}^{N_k} |\mathbf{r}_j(t) - \mathbf{r}_j(0)|^2 \right\rangle \quad (3)$$

where the sum is taken over all atoms of type k (k = Si,S,Li,I). Corresponding mean square displacements are provided in Fig. 5. These display the usual behavior, that is, at short times a ballistic regime sets in and behaves as $\langle r_k^2(t)\rangle \propto t^2$, whereas at long time the diffusive regime manifests by $\langle r_k^2(t)\rangle \propto t$. We note that the msd of the Li ions is much larger which provides a direct indication that the atomic motion is obviously decoupled between alkali ions and the network species (S,Si). With decreasing temperature, the onset of the diffusive regime appears at increasingly longer times. The self-diffusion D_k constant in the long-time limit is defined from the Einstein equation:

$$D_k = \frac{1}{6}\lim_{t\to\infty}\frac{\mathrm{d}\langle r_k^2(t)\rangle}{\mathrm{d}t}. \quad (4)$$

Note that even for T = 700 K, we can safely determine the Li and I diffusivities as the different $\langle r_k^2(t)\rangle$ display a well-defined diffusive regime that sets in for t >100 ps to 1 ns (Fig. 5). The behavior of the network species appears to be more contrasted (Fig. 5b, e, f) and for the binary LS liquids a clear plateau behavior sets in that extends up to the largest simulation time (1 ns). Here, the particles are obviously trapped in a cage-like motion. Diffusivity results now appear in Fig. 6 in an Arrhenius representation for both LS and LSI liquids (See also Table 3). We are not aware of any tracer diffusion measurements for the present thiosilicate systems but the obtained values are compatible with those measured in similar modified sulfide glasses [45–47]. Both LS and LSI liquids obviously do not follow the same dynamics, and while the reference LS systems leads to an obvious limited motion for the network species (S, Si, open symbols, broken lines) and a decoupling of Li and (Si,S) dynamics with differences in diffusivity by a factor of about 50, this is not the case for the LSI. Here, although one acknowledges a dominant motion for Li and I, all diffusivities are found to be nearly of the same order of magnitude, e.g. at 900 K one finds 9.01(5) cm^2 s^{-1} and 0.57(9) cm^2 s^{-1} for Li and Si, respectively. The origin of a

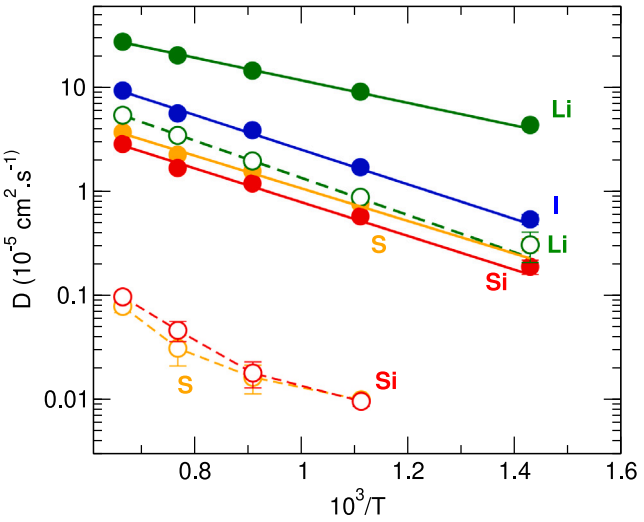

Fig. 6. Calculated diffusivity in LSI (filled symbols) and LS (open symbols): Li (green), S (orange), Si (red), I (blue).

Table 4
Activation energies E_A (in eV) of diffusivities and conductivity in LSI and LS liquids. Comparison with experimental data from Pradel and Ribes [17].

	D_{Li}	D_S	D_{Si}	D_I	σ	σ_{exp}
LSI	0.25	0.31	0.32	0.28	0.18	0.27 [17]
LS	0.35	0.64	0.61		0.28	0.25 [17]

similar diffusivity for all species in LSI liquids is related to the fact that the corresponding network is depolymerized in an increased fashion with respect to the reference LS liquid as quantified by the number of bridging sulfur atoms in the network (Table 2). This is in line with the general accepted picture that at fixed temperature diffusivity increases with network depolymerization or with an increasing number of non-bridging atoms [48]. Diffusivity is of activated (Arrhenius) type that is already evidenced by the representation (semi-log in 1/T), and corresponding activation energies E_A are given in Table 4. These highlight the reduced barriers for Li motion in LSI (0.25 eV) with respect to the reference LS system (0.35 eV), the network species leading to a diffusivity activation energies that are somewhat larger.

4.2. Loss of channel dynamics

The nature of the dynamics between LS and LSI is also governed by Li–Li correlations. By building on the analysis performed by Meyer et al. [49], one finds that the Li–Li partial structure factor $S_{LiLi}(k)$ (Fig. 8) exhibits a well-defined pre-peak at $k \simeq 1.05$ Å^{-1} in LS but not in LSI. The existence of this pre-peak is the signature that some ordering of Li ions takes place and involves a typical length scale [50] of $7.7/k_{PP} \simeq 7$-8 Å since the position r of the peak in real space is related to the position k of the corresponding peak in Fourier space by using the relation $kr \simeq 7.7$, which identifies the location of the first maximum of the spherical Bessel function $j_0(kr)$.

The existence of a typical pre-peak in alkali–alkali correlations in Fourier space is a typical feature observed in modified silicates [51,52] and also in certain thiosilicates [53], and is linked with the presence of preferential pathways for ion motion, termed in the literature as "channels" [54–57], and measured from quasi-elastic neutron scattering experiments [49,58]. Indeed, such alkali-rich regions with a characteristic length scale of ≃7 Å are found within a nearly frozen (thio)silica matrix, and result from the depolymerization of the structure [59] with alkali clustering emerging that lead to the percolation of alkali channels [60] for ≃20% Na_2O in binary sodium silicate glasses [57].

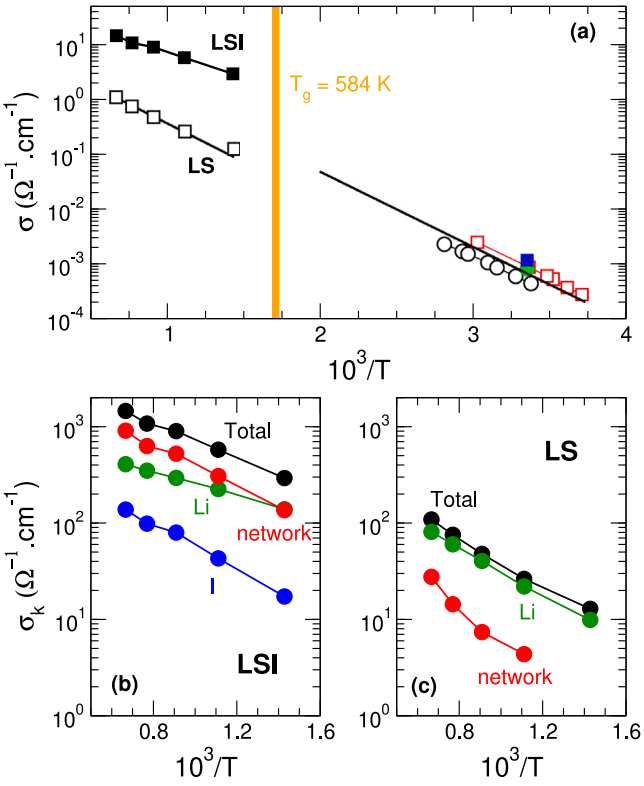

Fig. 7. (a) Calculated conductivity $\sigma(T)$ in LS (open boxes) and LSI (filled boxes) together with low temperature experimental data: LS (open circles [17]) and LSI (red boxes [17]; green circle [16] blue box [8]). The glass transition of LSI [17] is indicated. Calculated contribution of different structures to conductivity in LSI (b) and LS (c) liquids: total (black, same as panel a), σ_I contribution from iodine atoms (blue), σ_{Li} contribution from lithium atoms (green), and σ_N contribution from the network (Si,S) atoms (red, Eq. (7)).

In the present thiosilicates, the LS behavior (Fig. 8) is very close to the one found recently at a somewhat different Li content [53]. Here a pre-peak was found at ≃1.0 Å at various temperatures in the $50SiS_2$-$50Li_2S$. Conversely, no pre-peak is found in the LSI system which is an obvious indication that the channel dynamics is lost. An inspection of accumulated atomic snapshots (Fig. 8) permits to visualize the difference in atomic motion between both systems. In LS liquids, an obvious channel dynamics is acknowledged which manifests by well-separated regions of the simulation box for the motion of Li and the network species. This results from the polymerized network structure that is still maintained by some remaining BS atoms, i.e. the presence of Q^2 species (Table 2). On the opposite, the Li motion in LSI is possible inside the entire simulation box as the (Si,S) structure is made only of isolated Q^0 species and a limited number of pyrothiosilicate fragments (Q^1). As a result the typical correlating distance associated with the channel dynamics has vanished in $S_{LiLi}(k)$ of LSI (Fig. 8). Another consequence is that the Li–Li correlating distance in real space found at 3.01 Å (Fig. 2b) in LS is reduced with respect to LSI (3.57 Å) as more free space is available in the latter.

4.3. Conductivity

The conductivity (σ) as a function of temperature T can be obtained from the Nernst–Einstein equation [61]:

$$\sigma(T) = \lim_{t\to\infty} \frac{Ne^2}{6tVk_BT} \sum_{i,j} z_i z_j \left\langle [\mathbf{r}_i(t) - \mathbf{r}_i(0)][\mathbf{r}_j(t) - \mathbf{r}_j(0)] \right\rangle \quad (5)$$

where V is the volume of the simulation box, e is the elementary charge, z_i and z_j are the fractional charges of ions i and j of the

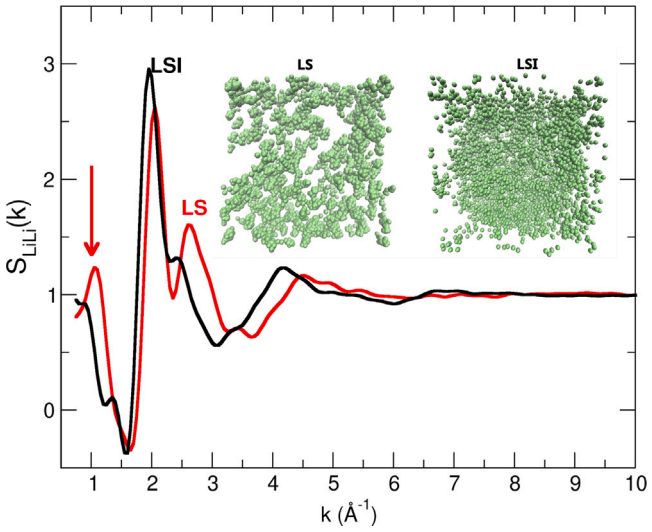

Fig. 8. Calculated Li–Li correlations $S_{LiLi}(k)$ in reciprocal space for LS (red) and LSI (black) systems. The arrow indicates the presence of a first sharp diffraction peak. The two atomic snapshots represent a slice (5 Å thickness) of LS and LSI liquids (900 K) representing accumulated frames of Li atoms over 100 ps with a frame frequency of 1 ps.

interaction potential, respectively. Here $\mathbf{r}_i(t)$ is the position of atom i, and the brackets $\langle\rangle$ denote ensemble averages. We note that cross (distinct) correlations ($i \neq j$) between the motions of the different atoms are negligible compared to self contributions so that only diagonal contributions ($i = j$) contribute. Corresponding data for $\sigma(T)$ (Eq. (5)) are represented in Fig. 7a in the liquid state where the simulated liquids can be safely equilibrated, and eventually compared to experimental measurements for LSI [8,16,17] and LS [17]. We first note that, as in experiments, LSI systems display a larger level of conduction when compared to LS and this highlights the usefulness of additives such as LiI (or LiCl) in these thiosilicate glasses in order to increase σ. Here it is found close to the glass transition (700 K) σ = 12.87 Ω^{-1} cm^{-1} and 293 Ω^{-1} cm^{-1} for LS and LSI, respectively. The data calculated in the liquid state, furthermore, appear to be compatible with those measured in the glass at $10^3/T$ >2.5 since the trends of the low- (experimental) and high-temperature (theoretical) can eventually connect together in the glass transition region. Both display obviously an Arrhenius behavior whose activation energies are provided in Table 4. Of particular interest is the fact that the fitted LSI activation energies from the simulations (0.18 eV) are lower than in LS (0.28 eV), in contrast with the measurements in the glassy state (0.25 eV versus 0.25 eV [17]). While the reduction of the simulated activation energies are compatible with the increased conductivity level in LSI, one should however keep in mind that there might be a so-called Arrhenius crossover in the glass transition region (here T_g = 306 °C for LSI [17]), which reflects the fact that, similarly to other glass-forming electrolytes [62–66], conductivity is enhanced once the underlying network softens with the reduction of viscosity. This might not only lead to conductivity jumps of the order of $\Delta\sigma$ = 10-10^3 Ω^{-1} cm^{-1} at T_g, followed by a possible departure from Arrhenius behavior but will also manifest by differences (experimental versus simulation) in activation energies E_A such as those displayed in Table 4. In fact, for a glass the rearrangement of Si–S bonds as the primary component of structural relaxation is essentially at rest. In such a virtually static matrix, ionic conductivity involves minor structural modification and is decoupled from the primary network relaxation, showing Arrhenius behavior with a given E_A. As temperature approaches the glass transition range, the primary relaxation is activated, leading to a complex temperature dependence present in the liquid, and possibly to a different E_A.

The detail of conductivity contributions reveals some interesting differences between LS and LSI (Figs. 7b and c). Here one splits Eq. (5) into contributions arising from the Li ions, from the network species (N), and from iodine anions, i.e. one focuses on different contributions σ_k (k = Li, I, N):

$$\sigma_k = \frac{e^2}{V k_B T} D_k(T) \tag{6}$$

where D_k is the self-diffusion constant of the species k. We can furthermore compute the conductivity component of the network species (Si,S) given by:

$$\sigma_N = \frac{e^2}{V k_B T}\left[D_{Si}(T) + D_S(T)\right] \tag{7}$$

In LS systems, the calculated conductivity results mainly from the Li ions (Fig. 7c) which contribute to about 75% to the total conductivity, the contribution of the network species being limited albeit increasing with temperature, as usually observed in high temperature liquids [56]. Conversely, the LSI liquid exhibits a substantial increase of σ as already acknowledged (Fig. 7a). While the Li contribution is not really different between both systems, this increase results essentially now from an important network contribution (Si,S) that is even dominant at high temperature in LSI. We can, thus, conclude that the obtained conductivity increase with doping results from an growing contribution of (Si,S) motions in LSI that is favored by the increased depolymerization of the network.

5. Discussion

We now provide some additional physical behavior from the atomic scale description and analysis, and target the lowest temperature considered for the dynamics, i.e. T = 700 K.

5.1. Free-volume increase

It is well-known that the increase of voids facilitates the motion of diffusing particles. An inspection of the free volume using a Voronoi tessellation permits to reveal profound differences once LiI is added into the network. The occupied volume can be determined for each particle from a Voronoi cell can is defined from the region of space closer to a given atom than any other particle. This is mathematically defined by requesting that for a given metric space (M, d) and a discrete set of atomic positions $\{s_1, s_2, \ldots\} \subset M$, the Voronoi cell of an atom fulfills

$$V(s_i) = \{x \in M |\ d(x, s_i) \leq d(x, s_j)\} \quad \forall i \neq j \tag{8}$$

Resulting distributions of the occupied volume V_i (i = Si,S,Li,I, Voronoi cell) are displayed in Fig. 9 for the doped glass (solid curves) together with the reference LS system (shaded distributions). Li and iodine atoms obviously occupy the largest volume due to their non-directional interactions, and for the doped systems such distributions are broad and centered at V_i = 30 and 35 Å^3, respectively. This indicates that both Li and I ions occupy essentially large volumes, in contrast with the network species. The bimodal distribution obtained for the Si species arises from the presence of two possible environments, i.e. a regular Si tetrahedra having either four sulfur atoms as neighbors, or tetrahedra containing a Si–I bond, at a somewhat larger distance (2.8 Å, see Fig. 2c). These lead to two different Voronoi volumes. As expected, for the reference glass, the Si distribution reduces to a sharp one at V_1 ≃15 Å^3 since there are 100% $SiS_{4/2}$ tetrahedra. Given the difference in density between both systems, it is instructive to rescale Fig. 9 with respect to ρ_0 (Fig. 10), and the effect of LiI doping clearly signals that the volume occupied by sulfur atoms reduces with LiI addition as a shift from an average $\rho_0 V_1$ ≃1.0 to 0.84 is acknowledged. This might leave more free space for carrier motion. We also calculate the free volume left for the Li motion which is nothing else then the system volume V minus the volume occupied by the network

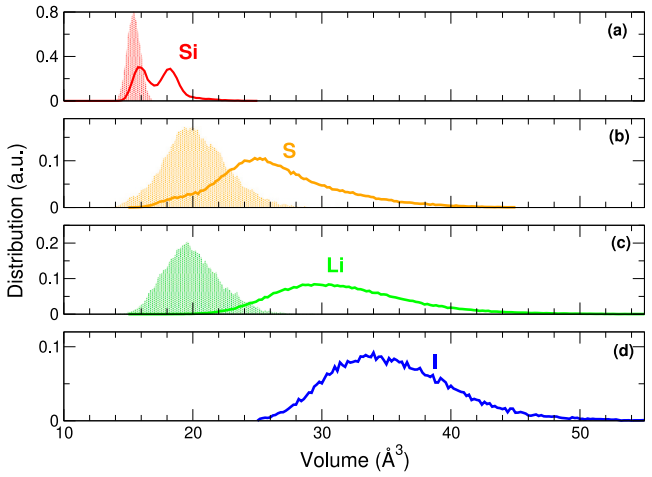

Fig. 9. Normalized Voronoi distribution for the various species involved at 700 K: Si (a), S (b), Li (c), and iodine (d). Solid curves correspond to the doped LSI system, whereas the shaded distributions correspond to the reference LS system.

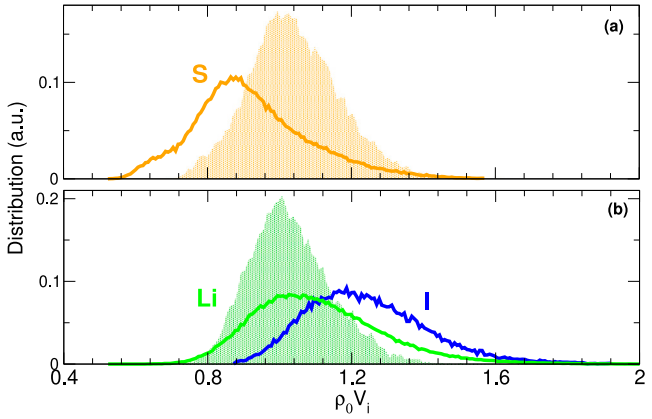

Fig. 10. Rescaled Voronoi distribution with respect to system density ρ_0 for S (orange, a), Li (green, b), and iodine (blue, b). Solid curves correspond to the doped system, whereas the shaded distributions correspond to the reference system. Here we have used ρ_0 = 0.051(3) Å^{-3} and ρ_0 = 0.035(5) Å^{-3} for LS and LSI respectively, which corresponds to the calculated values at zero pressure and 300 K (see above).

species (Si,S) and the iodine. The fraction of available free volume for ion motion can, indeed, be precisely calculated from the Voronoi distribution and is equal to 41.02% in the LS glass, i.e. close to the fraction calculated for a similar sulfide [38] (49,1% in $2Na_2S$-GeS_2). For the iodine system LSI, the fraction is equal to 53.4%, i.e. a substantial increase of free space is found and permits an enhanced ionic motion that is linked with the breakdown of the Li channels found in LS liquids.

5.2. Effect of atomic stresses

The link between stressed regions in the glass and ion motion has been recently emphasized [67]. Here we examine such a relationship by using the notion of "*stress per atom*" proposed by Thompson et al. [68] which builds on an atomic scale calculation of stress Σ_i via the virial approach. Previous investigations have used this local approach to quantify the extent of local instabilities in the glass structure [67,69]. One should remind that this stage that the virial has only a rigorous meaning once it is statistically averaged over an ensemble of particles, that is, once such a calculation is performed e.g. for the whole system leading to the system stress (or pressure) over the system volume. This framework provides an interesting means for the analysis of the local

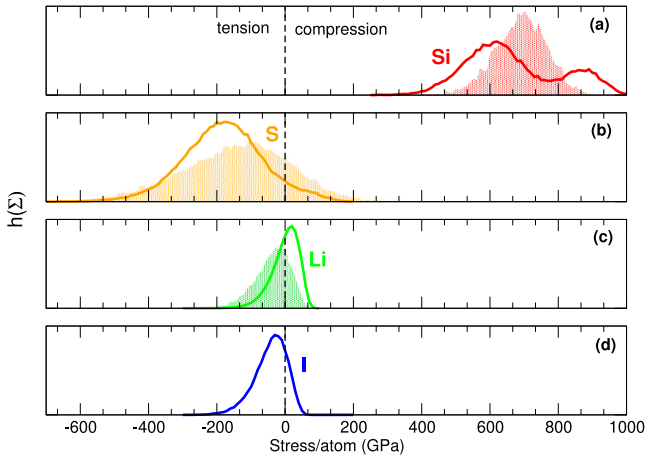

Fig. 11. Normalized atomic stress distribution h(Σ) for the various species involved at 700 K: Si (a), S (b), Li (c), and iodine (d). Solid curves correspond to the doped LSI system, whereas the shaded distributions correspond to the reference LS system.

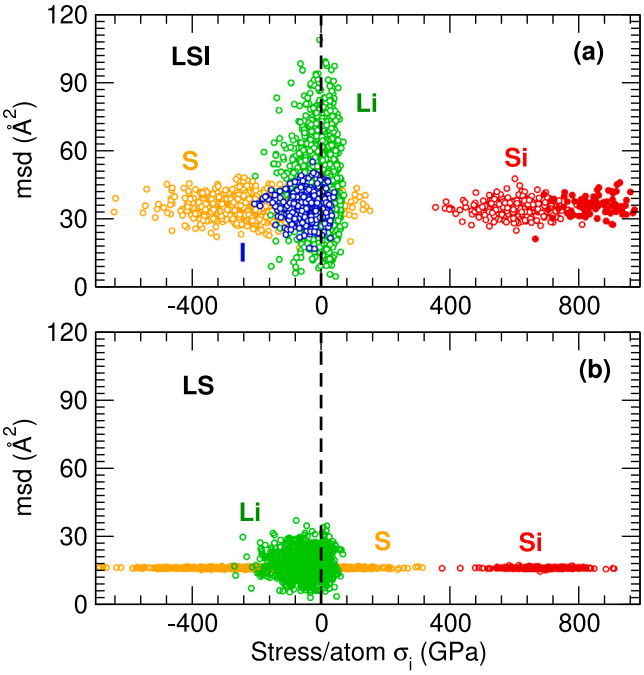

Fig. 12. Individual mean-square displacement of the different species at 700 K after 1 ns trajectory in LSI (a) and LS (b) liquids: Si (red), S (orange), Li (green), I (blue). Filled red circles correspond to Si atoms having a Si–I bond.

state of stress, compression (Σ_i <0) or tension (Σ_i> 0), experienced by each atom.

In Fig. 11, we represent such stress distributions for all species of the LS and LSI glasses. A certain number features clearly appear. Although the entire systems are at zero pressure, we find that Si and S atoms are systematically under tension and compression, respectively. While in the LS glass, the stress distribution for Si is centered at $\sigma \simeq$700 GPa, the LSI leads to a bimodal distribution which is the signature of the presence of two Si environments, pure $SiS_{4/2}$ tetrahedra and Si tetrahedra containing a Si–I bond. The former induces the larger stresses ($\Sigma \simeq$900 GPa, Fig. 11a) which underscores a tendency to Si–S bond compression that is balanced by a tendency for the S sulfur atoms to stretch the S–Li bonds (Fig. 11b). Interestingly, the Li and I atoms have a rather reduced stress distribution, close to zero, which means that the addition of an additive will not promote tensile and compressive

zones in the glass but will instead tend to reduce such zones. The stress variability can be quantified by the variance $v_\Sigma^2 = \langle \Sigma_i^2 \rangle - \langle \Sigma_i \rangle^2$ where one has, in principle, $\langle \Sigma_i \rangle \simeq 0$ as the overall system pressure is at zero. A computation of such a variance indicates, indeed, that one has $v_\Sigma = 43.2 \pm 0.5$ GPa and $v_\Sigma = 44.8 \pm 0.7$ GPa for LSI and LS, respectively. Thus, one can conclude that fluctuations in the glass are slightly reduced in the doped system, with ion dynamics possibly promoted by the absence of compressive or tensile stress barriers.

In order to establish a final correlation, we represent the individual mean-square displacements $|\mathbf{r}_j(t) - \mathbf{r}_j(0)|^2$ for each atom as a function of its corresponding stress (Fig. 12) which highlight the fact that mobile particle are those with zero stress and small size. Here one furthermore notes that the doping induces a reduction of tensile stresses around Li as the distribution $h(\Sigma)$ is found to shift to higher pressures from LS (Fig. 12b) to LSI (Fig. 12a) which has an obvious average zero stress in LSI.

6. Summary and conclusion

Here we have investigated the effect of an additive on the structural, dynamic and electric properties of thiosilicate glasses. A reference $0.6Li_2S$-$0.4SiS_2$ system and a doped $0.42Li_2S$-$0.28SiS_2$-0.3LiI system containing lithium iodide have been described from molecular dynamics simulations. The interest in such ternaries is driven by the important conductivity level which makes such alloys attractive for solid state battery applications. Previous attempts to describe such important systems for fast ion conductors trace back to the early 1990's, and were essentially arising from experimental studies [7,8,16]. In order to describe these glasses at the atomic scale, there has been need to establish a force-field for the classical molecular dynamics simulations and this has been performed by adding extra iodine related interactions to the initial lithium thiosilicate potential [19].

Results highlight the fact that LiI mostly dissolves in the glass structure, leading to extra lithium charge carriers, while also inducing the presence of Si–I in the first coordination shell of silicon. Such charge carriers, furthermore, contribute to an additional disruption of the reference LS glass as the Q^n speciation evolves significantly upon LiI addition from a broad Q^n distribution to a nearly 100% Q^0, together with a small presence of Q^1-Q^1 dimers. The dynamics of both liquids appear to be very different, driven by the possible vanishing of the channel-like dynamics in LS, and reveals a near decoupling of atomic motion between Li and network species in LS, while diffusivities differences are less than of one order of magnitude in the doped liquids. This induces a more important contribution to conductivity so that both Li and (Si,S) contribute almost equally to σ in $0.42Li_2S$-$0.28SiS_2$-0.3LiI. As the local stresses involved by Li and I are close to zero, the addition of LiI leads to reduction of the stress fluctuations in the structure. Other interesting ternary doped thiosilicates might be considered in the future along the same scheme, such as Li_2S–SiS_2-LiCl since such glasses seem to also be promising candidates [8] for solid state batteries.

CRediT authorship contribution statement

M. Micoulaut: Writing – review & editing, Writing – original draft, Methodology, Investigation, Funding acquisition, Formal analysis, Data curation, Conceptualization.

Declaration of competing interest

The authors declare the following financial interests/personal relationships which may be considered as potential competing interests: Matthieu Micoulaut reports financial support was provided by Fondation MAIF pour la recherche. If there are other authors, they declare that they have no known competing financial interests or personal relationships that could have appeared to influence the work reported in this paper.

Data availability

Data will be made available on request.

Acknowledgments

The author acknowledges support from Chaire d'Excellence Sorbonne Université - Universidad Autónoma de Mexico, and from Fondation MAIF pour la recherche. Supercomputing access to the cluster Romeo from Université de Reims Champagne-Ardenne is gratefully acknowledged. The author has abandoned the idea of being funded by the controversial ANR. Interactions and discussions with Louis-Martin Poitras, Andrea Piarristeguy, Søren Sørensen, Gerardo Naumis, Hugo Flores-Ruiz and Annie Pradel are also acknowledged.

References

[1] M. Weiss, R. Ruess, J. Kasnatscheew, Y. Levartovsky, N.R. Levy, P. Minnmann, L. Stolz, T. Waldmann, M. Wohlfahrt-Mehrens, D. Aurbach, et al., Fast charging of lithium-ion batteries: a review of materials aspects, Adv. Energy Mater. 11 (33) (2021) 2101126.

[2] J.-M. Tarascon, M. Armand, Issues and challenges facing rechargeable lithium batteries, Nature 414 (6861) (2001) 359–367.

[3] J. Wen, Y. Yu, C. Chen, A review on lithium-ion batteries safety issues: existing problems and possible solutions, Mater. Express 2 (3) (2012) 197–212.

[4] Z.A. Grady, C.J. Wilkinson, C.A. Randall, J.C. Mauro, Emerging role of non-crystalline electrolytes in solid-state battery research, Front. Energy Res. 8 (2020) 218.

[5] A. Hayashi, M. Tatsumisago, Sulfide-glass electrolytes for all-solid-state batteries, Encycl. Glass Sci. Technol. Hist. Cult. 2 (2021) 1125–1134.

[6] C. Dietrich, D.A. Weber, S.J. Sedlmaier, S. Indris, S.P. Culver, D. Walter, J. Janek, W.G. Zeier, Lithium ion conductivity in Li_2S–P_2S_5 glasses–building units and local structure evolution during the crystallization of superionic conductors Li_3PS_4, $Li_7P_3S_{11}$ and $Li_4P_2S_7$, J. Mater. Chem. A 5 (34) (2017) 18111–18119.

[7] J.H. Kennedy, Y. Yang, Glass-forming region and structure in SiS_2-Li_2S-LiX (X=Br, I), J. Solid State Chem. 69 (2) (1987) 252–257.

[8] J.H. Kennedy, Z. Zhang, Improved stability for the SiS_2-P_2S_5-Li_2S-LiI glass system, Solid State Ion. 28 (1988) 726–728.

[9] H. Wada, M. Menetrier, A. Levasseur, P. Hagenmuller, Preparation and ionic conductivity of new B_2S_3-Li_2S-LiI glasses, Mater. Res. Bull. 18 (2) (1983) 189–193.

[10] M. Ribes, B. Barrau, J. Souquet, Sulfide glasses: Glass forming region, structure and ionic conduction of glasses in Na_2S-XS_2 (X=Si; Ge), Na_2S- P_2S_5 and Li_2S-GeS_2 systems, J. Non-Cryst. Solids 38 (1980) 271–276.

[11] J. Malugani, G. Robert, Preparation and electrical properties of the $37Li_2S$-$18P_2S_5$-45LiI glass, Solid State Ion. 1 (5–6) (1980) 519–523.

[12] J. Kennedy, Ionically conductive glasses based on SiS_2, Mater. Chem. Phys. 23 (1–2) (1989) 29–50.

[13] A. Pradel, A. Piarristeguy, Thio and selenosilicates, sulfide and selenide counterparts of silicates: similarities and differences, C.R. Geosci. 354 (S1) (2022) 79–99.

[14] K. Noi, A. Hayashi, M. Tatsumisago, Structure and properties of the Na_2S–P_2S_5 glasses and glass–ceramics prepared by mechanical milling, J. Power Sources 269 (2014) 260–265.

[15] R.P. Rao, M. Seshasayee, Molecular dynamics simulation of ternary glasses Li_2S–P_2S_5–LiI, J. Non-Cryst. Solids 352 (30–31) (2006) 3310–3314.

[16] J.H. Kennedy, Z. Zhang, Further characterization of SiS_2-Li_2S glasses doped with Lithium Halide, J. Electrochem. Soc. 135 (4) (1988) 859.

[17] A. Pradel, M. Ribes, Electrical properties of lithium conductive silicon sulfide glasses prepared by twin roller quenching, Solid State Ion. 18 (1986) 351–355.

[18] K. Mori, K. Iwase, Y. Oba, K. Ikeda, T. Otomo, T. Fukunaga, Structural and electrochemical features of $(Li_2S)_x$ - $(SiS_2)_{100-x}$ superionic glasses, Solid State Ion. 344 (2020) 115141.

[19] L.-M. Poitras, M. Micoulaut, Establishment of an empirical force-field for crystalline and amorphous Li_2S- SiS_2 electrolytes, Phys. Rev. B 107 (21) (2023) 214205.

[20] J. Lee, A. Pradel, G. Taillades, M. Ribes, S. Elliott, Structural studies of glassy $(Li_2S)_{0.5}(SiS_2)_{0.5}$ by isotopic-substitution neutron diffraction, Phys. Rev. B 56 (17) (1997) 10934.

[21] B.T. Ahn, R.A. Huggins, Synthesis and lithium conductivities of Li_2SiS_3 and Li_4SiS_4, Mater. Res. Bull. 24 (7) (1989) 889–897.

[22] B.T. Ahn, R.A. Huggins, Preparation, structures and conductivities of Li_2SiS_3 phases, Mater. Res. Bull. 25 (3) (1990) 381–389.

[23] J. Saienga, S.W. Martin, The comparative structure, properties, and ionic conductivity of LiI+Li_2S+GeS_2 glasses doped with Ga_2S_3 and La_2S_3, J. Non-Cryst. Solids 354 (14) (2008) 1475–1486.

[24] J.H. Kennedy, S. Sahami, S.W. Shea, Z. Zhang, Preparation and conductivity measurements of SiS_2-Li_2S glasses doped with LiBr and LiCl, Solid State Ion. 18 (1986) 368–371.
[25] W. Rühl, Zur Struktur dünner, bei tiefer Temperatur kondensierter Salzschichten. I. Alkalihalogenide, Z. Phys. 143 (1956) 591–604.
[26] H. Ott, Die Raumgitter der Lithiumhalogenide, Physikalische Zeitschrift 24 (1923) 209–213.
[27] O. Hassel, H. Kringstad, Kristallbau von Tetrahalogeniden leichterer Elemente. II, Z. Phys. Chemie 15 (1) (1932) 274–280.
[28] T. Klapoetke, J. Passmore, Sulfur and selenium iodine compounds: from non-existence to significance, Acc. Chem. Res. 22 (7) (1989) 234–240.
[29] J. Passmore, G. Sutherland, P. Taylor, T.K. Whidden, P.S. White, Preparations and x-ray crystal structures of iodo-cyclo-heptasulfur hexafluoroantimonate (V) and hexafluoroarsenate (V), S_7ISbF_6 and S_7IAsF_6, Inorg. Chem. 20 (11) (1981) 3839–3845.
[30] J.D. Gale, A.L. Rohl, The general utility lattice program (GULP), Mol. Simul. 29 (5) (2003) 291–341.
[31] J.D. Gale, Empirical potential derivation for ionic materials, Phil. Mag. B 73 (1) (1996) 3–19.
[32] L.T. Kong, Phonon dispersion measured directly from molecular dynamics simulations, Comput. Phys. Comm. 182 (10) (2011) 2201–2207.
[33] M. Micoulaut, Structure of densified amorphous germanium dioxide, J. Phys.: Condens. Matter 16 (10) (2004) L131.
[34] M. Micoulaut, I. Pethes, P. Jóvári, L. Pusztai, M. Krbal, T. Wágner, V. Prokop, Š. Michalik, K. Ikeda, I. Kaban, Structural properties of chalcogenide glasses and the isocoordination rule: Disentangling effects from chemistry and network topology, Phys. Rev. B 106 (1) (2022) 014206.
[35] M. Kassem, T. Bounazef, A. Sokolov, M. Bokova, D. Fontanari, A.C. Hannon, I. Alekseev, E. Bychkov, Deciphering fast ion transport in glasses: A case study of sodium and silver vitreous sulfides, Inorg. Chem. 61 (32) (2022) 12870–12885.
[36] L. Cai, P. Boolchand, Nanoscale phase separation of GeS2 glass, Phil. Mag. B 82 (15) (2002) 1649–1657.
[37] S. Chakraborty, P. Boolchand, M. Micoulaut, Structural properties of Ge-S amorphous networks in relationship with rigidity transitions: An ab initio molecular dynamics study, Phys. Rev. B 96 (9) (2017) 094205.
[38] M. Micoulaut, A. Piarristeguy, O. Masson, L.-M. Poitras, R. Escalier, A. Kachmar, A. Pradel, Quantitative assessment of network depolymerization in archetypal superionic glasses and its relationship with ion conduction: A case study on Na_2S- GeS_2, Phys. Rev. B 108 (14) (2023) 144205.
[39] F. Wang, P. Boolchand, K. Jackson, M. Micoulaut, Chemical alloying and light-induced collapse of intermediate phases in chalcohalide glasses, J. Phys.: Condens. Matter 19 (22) (2007) 226201.
[40] M. Micoulaut, R. Kerner, The structure of lithium silicon sulphide glass systems, J. Phys.: Condens. Matter 9 (12) (1997) 2551.
[41] H. Eckert, J.H. Kennedy, A. Pradel, M. Ribes, Structural transformation of thiosilicate glasses: ^{29}Si MAS-NMR evidence for edge-sharing in the system Li_2S - SiS_2, J. Non-Cryst. Solids 113 (2–3) (1989) 287–293.
[42] A. Pradel, G. Taillades, M. Ribes, H. Eckert, ^{29}Si NMR structural studies of ionically conductive silicon chalcogenide glasses and model compounds, J. Non-Cryst. Solids 188 (1–2) (1995) 75–86.
[43] H. Maekawa, T. Maekawa, K. Kawamura, T. Yokokawa, The structural groups of alkali silicate glasses determined from ^{29}Si MAS-NMR, J. Non-Cryst. Solids 127 (1) (1991) 53–64.
[44] Y. Tokuda, T. Uchino, T. Yoko, Vibrational dynamics of glassy SiS_2 on the basis of molecular orbital calculations, J. Non-Cryst. Solids 282 (2) (2001) 256–264.
[45] E. Bychkov, Tracer diffusion studies of ion-conducting chalcogenide glasses, Solid State Ion. 136 (2000) 1111–1118.
[46] I. Alekseev, D. Fontanari, A. Sokolov, M. Bokova, M. Kassem, E. Bychkov, Ionic conductivity and tracer diffusion in glassy chalcogenides, vol. 1, Singapore, World Scientific, 2020.
[47] M. Thomas, N.L. Peterson, E. Hutchinson, Tracer diffusion and electrical conductivity in sodium-rubidium silicon sulfide glasses, J. Am. Ceram. Soc. 68 (2) (1985) 99–104.
[48] H. Ni, H. Hui, G. Steinle-Neumann, Transport properties of silicate melts, Rev. Geophys. 53 (3) (2015) 715–744.
[49] A. Meyer, J. Horbach, W. Kob, F. Kargl, H. Schober, Channel formation and intermediate range order in sodium silicate melts and glasses, Phys. Rev. Lett. 93 (2) (2004) 027801.
[50] P.S. Salmon, Real space manifestation of the first sharp diffraction peak in the structure factor of liquid and glassy materials, Proc. R. Soc. Lond. Ser. A Math. Phys. Eng. Sci. 445 (1924) (1994) 351–365.
[51] C. Angell, P. Cheeseman, S. Tamaddon, Computer simulation studies of migration mechanisms in ionic glasses and liquids, Le J. Phys. Colloques 43 (C9) (1982) C9–381.
[52] G. Greaves, EXAFS and the structure of glass, J. Non-Cryst. Solids 71 (1–3) (1985) 203–217.
[53] S.S. Sørensen, M.M. Smedskjaer, M. Micoulaut, Evidence for complex dynamics in glassy fast ion conductors: The case of sodium thiosilicates, J. Phys. Chem. B 127 (47) (2023) 10179–10188.
[54] T. Voigtmann, J. Horbach, Slow dynamics in ion-conducting sodium silicate melts: Simulation and mode-coupling theory, Europhys. Lett. 74 (3) (2006) 459.
[55] E. Sunyer, P. Jund, R. Jullien, Characterization of channel diffusion in a sodium tetrasilicate glass via molecular-dynamics simulations, Phys. Rev. B 65 (21) (2002) 214203.
[56] M. Bauchy, M. Micoulaut, From pockets to channels: Density-controlled diffusion in sodium silicates, Phys. Rev. B 83 (18) (2011) 184118.
[57] P. Jund, W. Kob, R. Jullien, Channel diffusion of sodium in a silicate glass, Phys. Rev. B 64 (13) (2001) 134303.
[58] A. Meyer, F. Kargl, J. Horbach, Channel diffusion in sodium silicate melts, Neutron News 23 (3) (2012) 35–37.
[59] M. Micoulaut, Amorphous materials: Properties, structure, and durability: Constrained interactions, rigidity, adaptative networks, and their role for the description of silicates, Am. Mineral. 93 (11–12) (2008) 1732–1748.
[60] H. Nesbitt, G. Henderson, G. Bancroft, R. Ho, Experimental evidence for Na coordination to bridging oxygen in na-silicate glasses: Implications for spectroscopic studies and for the modified random network model, J. Non-Cryst. Solids 409 (2015) 139–148.
[61] J.-P. Hansen, I.R. McDonald, Theory of Simple Liquids: With Applications to Soft Matter, Academic Press, 2013.
[62] D. Golodnitsky, E. Strauss, E. Peled, S. Greenbaum, On order and disorder in polymer electrolytes, J. Electrochem. Soc. 162 (14) (2015) A2551.
[63] C.-H. Tu, L. Veith, H.-J. Butt, G. Floudas, Ionic conductivity of a solid polymer electrolyte confined in nanopores, Macromolecules 55 (4) (2022) 1332–1341.
[64] M. Aniya, M. Ikeda, Arrhenius crossover phenomena and ionic conductivity in ionic glass-forming liquids, physica status solidi (b) 257 (11) (2020) 2000139.
[65] M. Malki, V. Magnien, O. Pinet, P. Richet, Electrical conductivity of iron-bearing silicate glasses and melts. Implications for the mechanisms of iron redox reactions, Geochim. Cosmochim. Acta 165 (2015) 137–147.
[66] H. Fan, L. Del Campo, V. Montouillout, M. Malki, Ionic conductivity and boron anomaly in binary lithium borate melts, J. Non-Cryst. Solids 543 (2020) 120160.
[67] Y. Yu, M. Wang, M.M. Smedskjaer, J.C. Mauro, G. Sant, M. Bauchy, Thermometer effect: origin of the mixed alkali effect in glass relaxation, Phys. Rev. Lett. 119 (9) (2017) 095501.
[68] A.P. Thompson, S.J. Plimpton, W. Mattson, General formulation of pressure and stress tensor for arbitrary many-body interaction potentials under periodic boundary conditions, J. Chem. Phys. 131 (15) (2009).
[69] W. Song, X. Li, B. Wang, N. Anoop Krishnan, S. Goyal, M.M. Smedskjaer, J.C. Mauro, C.G. Hoover, M. Bauchy, Atomic picture of structural relaxation in silicate glasses, Appl. Phys. Lett. 114 (23) (2019).